Applied Energy 339 (2023) 120959

Contents lists available at ScienceDirect

Applied Energy

journal homepage: www.elsevier.com/locate/apenergy

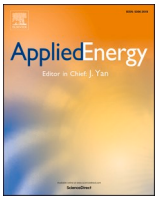

System efficiency and power assessment of the all-aqueous copper thermally regenerative ammonia battery

Nicholas R. Cross [a], Matthew J. Rau [b], Serguei N. Lvov [c,d,e], Christopher A. Gorski [f], Bruce E. Logan [a,f], Derek M. Hall [c,d,*]

[a] Department of Chemical Engineering, Pennsylvania State University, University Park, PA 16802, USA
[b] Department of Mechanical and Aerospace Engineering, The George Washington University, Washington, DC 20052, USA
[c] The EMS Energy Institute, Pennsylvania State University, University Park, PA 16802, USA
[d] Department of Energy and Mineral Engineering, Pennsylvania State University, University Park, PA 16802, USA
[e] Department of Materials Science and Engineering, Pennsylvania State University, University Park, PA 16802, USA
[f] Department of Civil and Environmental Engineering, Pennsylvania State University, University Park, PA 16802, USA

HIGHLIGHTS

- Membrane conductivity was the primary driver of power density for the Cu_{aq}-TRAB.
- Theoretical energy efficiency limits were established for a range of operating conditions.
- Volumetric footprint of Cu_{aq}-TRAB relative to power output of a natural gas turbine was estimated.

ARTICLE INFO

Keywords:
Low-grade waste heat
Thermally regenerative battery
Flow battery
Energy efficiency

ABSTRACT

Thermally regenerative ammonia batteries (TRABs) use low-temperature (T < 100 °C) heat to provide stationary energy and power with higher power densities and efficiency relative to other waste heat devices. TRABs are an active area of research in waste heat devices, but currently there is little consensus on what aspect of the system is limiting TRAB performance and what maximum efficiencies are possible. Experiments and numerical models were used here to examine the sensitivity of the battery and distillation column in a TRAB system to key operating variables, thereby establishing practical limits and identifying focus areas for improving performance. Battery power was eight times more sensitive to ohmic losses than kinetic and mass transfer losses, regardless of the operating temperature, and the peak power density was simulated to be 18.8 mW cm^{-2} at 75 °C. Theoretical energy efficiency limits were defined for a series of ammonia concentrations and operating pressures, ranging from 5 – 12%, which is 2–3 times higher than previous experimental estimations. Atmospheric pressure column operation used a larger amount of waste heat compared to sub-atmospheric pressure. It is estimated that the volume of the battery would take up 9.2 m^3 for every 1% of the power output of a natural gas turbine, but with realistic improvements to cell conductivity, the size would reduce to 2.5 m^3. The results presented in this work will help streamline future development by focusing on minimizing ohmic losses and provide specific data for full system evaluation of future TRABs.

1. Introduction

It is estimated that there is roughly 262 EJ of low-temperature (T < 100 °C) waste heat available around the world, with over half of it being produced at stationary sources in the power generation and industrial sectors [1]. Many different devices such as thermoelectrics and heat pipes are being considered to generate power from low-grade heat, but they have low power densities and cannot store energy [2]. Recent reviews have demonstrated that thermally regenerative electrochemical cycles, thermos-electrochemical cells, and thermally regenerative batteries (TRBs) have relatively high efficiencies and power densities while also being able to store energy, with TRBs having the best efficiency and power to date [3–8]. TRBs use ligand chemistry to modify the

* Corresponding author at: Department of Energy and Mineral Engineering, Pennsylvania State University, University Park, PA 16802, USA.
E-mail address: dmh5373@psu.edu (D.M. Hall).

https://doi.org/10.1016/j.apenergy.2023.120959
Received 3 January 2023; Received in revised form 14 February 2023; Accepted 5 March 2023
Available online 28 March 2023

Nomenclature

Variables

a	Activity coefficient (–)
c	Concentration (mol L^{-1})
D	Diffusion coefficient (m^2 s^{-1})
E	Potential (V)
$ECSA$	Active specific surface area (m^{-1})
F	Faraday's constant (C mol^{-1})
j_0	Exchange current density (mA cm^{-2})
K	Electrode permeability (m^2)
n	Number of electrons (–)
p	Fluid pressure (MPa)
Q	Power (W)
R	Molar gas constant (J mol^{-1} K^{-1})
T	Temperature (K)
u	Electrolyte inflow velocity (m s^{-1})
$\hat{u}$	Ideal energy density (Wh L^{-1})
$\dot{V}$	Volumetric flow rate (m^3 s^{-1})
α	Transfer coefficient (–)
ε	Electrode porosity (%)
η	Efficiency (%)
μ	Fluid dynamic viscosity (Pa s)
ρ	Fluid density (kg m^{-3})

Superscripts

0	Standard

Subscripts

a	Anolyte/Anode
c	Catholyte/Cathode
heat	Thermal
i	Species
init	Initial
o	Oxidized
out	Outlet
r	Reduced
tot	Total

equilibrium potential of a single redox reaction thereby creating a potential difference between two otherwise identical electrolytes. These electrolytes are stored in external tanks and pumped into the reactor stack to undergo redox reactions that store or provide electrical energy. One electrolyte will contain a ligand that can be thermally recharged using the low temperature waste heat through a process such as flash or continuous distillation. The most commonly used ligand is ammonia; however, ethylenediamine and acetonitrile-based systems have also been demonstrated. Both ethylenediamine and acetonitrile can provide some battery performance improvements but have additional limitations such as the formation of azeotropes with water (which increases the complexity of battery recharging), lower solubility limits, increased pumping losses, and greater conductivity losses [9–12].

The metals and supporting electrolytes used in thermally regenerative ammonia batteries (TRABs) are critical to stability and performance. TRABs that are based on reversible solid copper deposition and ammonia electrolytes have been extensively studied [13–16] but suffer from thermodynamic instability of solid copper due to irreversible losses caused by metal salt precipitation in the presence of ammonia, which drives down coulombic efficiency [17–19]. Using silver instead of copper avoids metal losses due to precipitation and therefore had high coulombic efficiency [20], but higher material costs and issues with deposition uniformity [21] limit the potential of this approach. Bimetallic TRABs using zinc and copper metal can significantly increase the power density of the battery as a result of large potentials during discharge. However, this chemistry has lower coulombic and energy efficiencies because copper-ammonia stability is not addressed, and the system design is more complex with multiple distillation steps and an electric recharging step [22–26]. Purging the electrolytes of oxygen using an inert gas and changing the anions to bromide, a weak field ligand, from nitrate and sulfate to stabilize Cu(I) rather than Cu(0) resulted in a new TRAB (referred to as the Cu_{aq}-TRAB) that avoids these problems, producing a high coulombic efficiency, power density, energy density, and thermal efficiency relative to previous single-metal TRAB chemistries [27,28].

Thermally regenerative batteries are designed to use low temperature heat for the thermal separation and therefore, there have been previous TRAB investigations to demonstrate the impact of temperature on battery performance with results showing moderate power increases with little energy density losses [13,25,29]. Due to low membrane conductivity in TRAB electrolytes, elevated temperature could help increase power because conductivity usually increases with temperature. The fluid temperature and pressure have also been shown to impact the energy required for thermal separation of ammonia from the anolyte [25,30–32]. However, basic relationships between battery temperature, electrolyte composition and energy required for thermal separation have yet to be determined and these aspects are of high importance because they impact both power density and energy efficiency. Recent work completed scaling analysis of a metal-based Cu-TRAB to compare its power output to an organic Rankine cycle (ORC) [32] and demonstrated that the TRAB would have lower power than the ORC. However, this analysis does not consider the amount of space and therefore equipment that each system would require for implementation which is pertinent for considerations of capital expenditures and geographical footprint. Therefore, additional analysis should be done for proper comparison between TRABs and ORCs.

In this work, we developed a model supported by experiments to conduct a sensitivity analysis of battery power output at and above room temperature to quantify sources of kinetic, ohmic, and mass transfer losses to identify critical research directions that can realize significant gains in Cu_{aq}-TRAB performance. The sensitivity of the Cu_{aq}-TRAB to kinetic, ohmic, and mass transfer losses was quantified over a range of battery operating temperatures. To improve full system evaluation of TRABs, previous models of the thermal recharging process were expanded upon to estimate energy requirements for a range of ammonia concentrations and operating temperatures to define theoretical efficiency limits of the Cu_{aq}-TRAB cycle more clearly. Furthermore, we demonstrated the current volumetric footprint of the Cu_{aq}-TRAB in comparison to a natural gas turbine and project how much smaller the footprint could become with battery performance gains. This work clearly demonstrates methods that should be used to streamline performance assessments of all TRBs, not just the Cu_{aq}-TRAB, and defines methods upon which technology improvements should be evaluated.

2. Materials and methods

2.1. Materials

Electrolyte solutions were created using ammonium bromide (99%, Alfa Aesar), copper (I) bromide (98%, Alfa Aesar), copper (II) bromide (99%, Acros Organics), and deionized water (<1 MΩcm, Aqua Solutions, RODI-T2). The source of ammonia was a 28 wt% ammonium hydroxide solution (Sigma-Aldrich). All electrolytes were purged with argon (99.997%, Praxair) to prevent undesired oxidation of the copper during testing. Nafion 117 was the separator for all full cell tests, and the electrodes were carbon felt (AvCarb G300A); both were used as

received.

2.2. Electrochemical characterization

All full cell tests were run using a 25 cm^2 column-pin flow field (FuelCellStore) on a graphite plate in a flow-through configuration, similar to previous work [28]. The catholyte and anolyte (100 mL each) were pumped into the reactor stack at 50 mL min^{-1} using a peristaltic pump. Electrochemical characterizations were completed using a Gamry Reference 3000. Polarization curves were obtained by linearly sweeping the cell potential from the open circuit potential to 0 V at a sweep rate of 10 mV s^{-1}. Discharge curves were conducted at 10 mA cm^{-2} with a cutoff voltage of 0.35 V. The temperature of the system was controlled by heating the electrolyte tanks and steel reactor endplates (Fig. S1a). The electrolyte tanks were stored in an oil bath with a built-in heater and temperature control system (ThermoScientific). A thermocouple was inserted into the graphite flow field to monitor the temperature inside the electrochemical cell, and the thermocouple was connected to a controller that modulated the heat output of resistive heating elements that were adhered to the steel endplates to control the cell temperature ($T \pm 1$ °C).

2.3. Battery numerical model

A 3-dimensional numerical model was created using COMSOL Multiphysics to simulate polarization curves and assess the sensitivity of the Cu_{aq}-TRAB to polarization losses (ohmic, mass transfer, and charge transfer) for a range of operating temperatures. The model was composed of three domains: 1) porous positive electrode, 2) membrane, and 3) porous negative electrode, with a simplified pin-column structure in each electrode chamber to capture the influence of the flow field on system performance (Fig. S1b). Complete details on the equations used to construct the model are in the supplementary information. The model used symmetric boundary conditions on the external walls parallel to the flow path to reduce the model size and computational time. The model depth was 0.8 cm in comparison to the actual electrode depth of 5 cm. Current and power density results were scaled linearly to account for the smaller projected area. The membrane was modeled as a linear ohmic drop with a fixed conductivity acting as a sink/source of NH_4^+ ions to maintain electroneutrality within each electrode chamber. The electrodes were assumed to be homogenous porous media of uniform porosity and permeability and were assumed to be isothermal at the desired operating temperature. It was found that active surface area and permeability of the electrodes had very little impact on the polarization curves over possible ranges of values of these variables (Fig. S2). Laminar, incompressible Brinkman and continuity equations governed the fluid flow through the porous electrode [33]. A no-slip boundary condition was imposed at all non-symmetry boundary condition walls (flow field and membrane). The electrolyte flow path was modelled through the porous electrode to obtain a steady-state solution of fluid flow in the absence of electrochemical transport (just Eqs. S1 and S2). This solution was then used in the electrochemical model as a fixed flow path/boundary layer distribution in the electrode. It was assumed that the change in concentrations produced by the electrochemical reactions would not change the flow distribution. This method reduced total computational time by not having to solve the fluid mechanics and electrochemistry simultaneously. Fluid parameters used in the simulations were measured experimentally (Table 1).

The flux and concentration change of all species in the electrode channels were governed by the conservation of mass and convection–diffusion equations [34]. We estimated the diffusion coefficients of all copper species using the Levich equation for a rotating disk electrode system and data from our previous work (Table 2) [27,35]. It was assumed these would not change significantly with temperature, and this assumption was shown to have no impact on the power curves (Fig. S2c). Diffusion coefficients of ammonium, bromide, and ammonia species at all temperatures were estimated using tabulated molar conductivity data [36,37].

Table 1
Fluid flow parameters.

Description	Variable	Value	Units
Fluid pressure	p	0.1013	MPa
Catholyte density (25, 50, 75 °C)	ρ_c	1270, 1271, 1254 [a]	kg m^{-3}
Anolyte density (25, 50, 75 °C)	ρ_a	1202, 1149, 1152 [a]	kg m^{-3}
Catholyte dynamic viscosity (25, 50, 75 °C; x 10^{-4})	μ_c	9.05, 6.40, 4.89 [a]	Pa s
Anolyte dynamic viscosity (25, 50, 75 °C; x 10^{-4})	μ_a	9.87, 6.62, 5.05 [a]	Pa s
Electrolyte normal inflow velocity	u	0.002	m s^{-1}
Fluid outlet pressure	p_{out}	0	MPa
Electrode permeability	K	1×10^{-11} [b]	m^2
Electrode porosity	ε	90 [b]	%

[a] Measured value.
[b] Estimated parameter, see Fig. S2.

Table 2
Electrolyte properties.

Description	Variable	Values	Units
Cu catholyte species diffusion coefficient (I, II; x 10^{-10})	$D_{CuI,c}$, $D_{CuII,c}$	9.16, 7.52 [a]	m^2 s^{-1}
Cu anolyte species diffusion coefficient (I, II; x 10^{-10})	$D_{CuI,a}$, $D_{CuII,a}$	4.18, 9.10 [a]	m^2 s^{-1}
NH_4^+ diffusion coefficient (25, 50, 75 °C; x 10^{-10})	D_{NH4+}	9.26, 12.3, 14.5 [b]	m^2 s^{-1}
Br^- diffusion coefficient (25, 50, 75 °C; x 10^{-10})	D_{Br-}	9.84, 13.1, 15.4 [b]	m^2 s^{-1}
NH_3 diffusion coefficient (25, 50, 75 °C; x 10^{-9})	D_{NH3}	1.60, 2.37, 3.14[b]	m^2 s^{-1}
Cu initial concentration	$c_{Cu,init}$	0.5	mol L^{-1}
NH_4^+ bulk/initial concentration	$c_{NH4+,init}$	5	mol L^{-1}
Br^- bulk/initial concentration	$c_{Br-,init}$	6	mol L^{-1}
NH_3 initial concentration	$c_{NH3,init}$	4	mol L^{-1}

[a] Estimated using[27].
[b] Estimated using[37].

We modeled the kinetics within the porous electrode using the linearized form of the Butler-Volmer equation (Eq. S6). We assumed that the sum of the transfer coefficients for each reaction was one. The local current density was scaled to the current output of the electrode through the active specific surface area. The electrochemical reactions in each electrolyte were assumed to be single-step, one-electron redox reactions that did not impact the concentration of free ligand in the electrolyte because of the high concentration of ligand relative to copper ions. The positive electrode half-reaction can be written as

$$CuBr_2 + e^- \leftrightarrow CuBr_2^-. \quad (1)$$

The negative electrode half-reaction can be written as

$$Cu(NH_3)_3^{2+} + e^- \leftrightarrow Cu(NH_3)_3^+. \quad (2)$$

While the degree of copper complexation (3) is an estimation based off previous calculations [27], there is no impact on the voltage as a result of how we defined the Nernst equation and because standard potential values were measured experimentally. The equilibrium potential of each electrode was modelled using the Nernst equation, which for the positive electrode was

$$E_{eq,c} = E_c^0 + \frac{RT}{nF}\left(\frac{ac_{Cu,co}}{ac_{Cu,cr}}\right). \quad (3)$$

The negative electrode was written as

$$E_{eq,a} = E_a^0 + \frac{RT}{nF}\left(\frac{ac_{Cu,ao}}{ac_{Cu,ar}}\right), \quad (4)$$

where E_{eq} is the equilibrium potential, E^0 is the standard potential of a reaction, n is the number of electrons transferred, a is the activity coefficient, c is the species bulk concentration, subscript c denotes a species in the catholyte, subscript a denotes a species in the anolyte, subscript o is an oxidized species, and subscript r is a reduced species [35]. All activity coefficients were assumed to be one because the initial state of charge was used to match the open circuit potential. The initial state of charge of the battery (dictating the ratio of oxidized to reduced copper species in each electrolyte) was 99.5%, and this was the only value that was modified to fit the model results to the experiment. This choice is what enabled us to assume the activity coefficients were one because the concentration of each species does not change significantly during a polarization test and because the charge number of each species is similar and largely cancels out in the Nernst equation [38]. The standard potential of each reaction was measured using a three-electrode setup at a range of temperatures using a temperature controlled mineral oil bath (Table 3) [39].

To estimate cell conductivity within the electrochemical reactor, we measured the ohmic resistance of the full cell for a range of temperatures using electrochemical impedance spectroscopy. Given the high conductivity of the non-membrane components of the cell, it was assumed that the ohmic resistance was primarily due to the membrane resistance and contact resistances between the membrane, electrodes, and flow fields. Using the wetted thickness of the membrane (212 μm [41]) and the projected geometric area of the membrane, the cell conductivity was 0.233, 0.282, and 0.334 S m^{-1} at 25, 50, and 75 °C, respectively. Our experimental setup was only able to sustain a temperature of 65 °C at the flow cell, thus the conductivity at 75 °C was an extrapolation based on conductivities measured at lower temperatures, and the results presented for 75 °C are a projection.

The numerical model was used to conduct a sensitivity analysis to evaluate the contributions of ohmic, mass transfer, and kinetic losses to battery performance by modifying cell conductivity, flow rate, and exchange current density. The "baseline" parameters for comparing performance were those measured experimentally at each temperature and a flow rate of 20 mL min^{-1}. To evaluate the sensitivity of the Cu_{aq}-TRAB, flow rates of 10 and 50 mL min^{-1} were used, and the membrane conductivity and the exchange current density were varied by ±20% relative to experimentally measured values. These independent variables were chosen because they regulate ohmic, mass transfer, and kinetic losses in flow batteries, and they can be manipulated relatively easily (e.g. changing membranes, increasing pumping rate, changing catalysts). A range of ±20% is reasonable based on previous investigations that have measured the membrane conductivity with different custom membranes [42] and rate constants for multiple ligands at a range of concentrations [27]. Polarization curves were modeled for each case by increasing the applied current to the cell in discrete steps, with the model then estimating the resultant cell voltage at each applied current density. These were turned into power curves by $p = iV$, where p is the power density, i is the current density, and V is the cell potential difference (voltage). The current density was normalized to the projected geometric area of the cell.

Table 3
Electrode kinetic and thermodynamic parameters.

Description	Variable	Value	Units
Cathode exchange current density	$j_{0,c}$	29 [a]	mA cm^{-2}
Anode exchange current density	$j_{0,a}$	8.4 [a]	mA cm^{-2}
Cathode cathodic transfer coefficient	$\alpha_{c,c}$	0.33 [a]	–
Anode cathodic transfer coefficient	$\alpha_{c,a}$	0.25 [a]	–
Specific surface area	SSA	44,010[b]	m^2 m^{-3}
Anode standard potential (25, 50, 75 °C) vs. SHE	E_c^0	0.53, 0.54, 0.55[c]	V
Anode equilibrium potential (25, 50, 75 °C) vs. SHE	E_a^0	−0.21, −0.17, −0.12[c]	V

[a] See ref. [27].
[b] See ref. [40].
[c] Measured parameter.

2.4. Distillation column numerical model

For the thermal regeneration of the battery electrolytes, only the ammonia-water separation was taken into account due to its energy requirement being much higher than the energy required for separation of the ammonia from the copper complex [15]. Aspen HYSYS V12.1 was used to estimate the energy requirement of ammonia-water separation, with the Peng-Robinson equation of state being used for the thermodynamic properties and binary coefficients of the ammonia-water mixture [43]. We modeled the distillation column to have 10 stages with the feed at stage 5 (Fig. 1). The condenser operated under full reflux, therefore sending all the liquid back to the column, with a vapor product stream of >99% NH_3 venting before the condenser. The bottoms stream was required to have a water purity of 99.9% water. The reflux ratio (defined as the ratio of the amount of distillate going back through the condenser to the amount of distillate leaving as product) was minimized to decrease condenser duty without sacrificing the purity of the distillate NH_3 product stream. After the distillation column, both the distillate and bottoms outlet streams were sent through heat exchangers whose heat inputs were adjusted to set the outlet temperature of product streams to be equal to the temperature of the inlet stream of the distillation column. The operating pressure and pressure drop of the sub-atmospheric column and all streams were kept consistent with previous TRAB distillation column models of 0.24 atm [32,44]. The atmospheric column had all streams at atmospheric pressure and the pressure drop across the column was the same as the sub-atmospheric column, to be consistent with previous models.

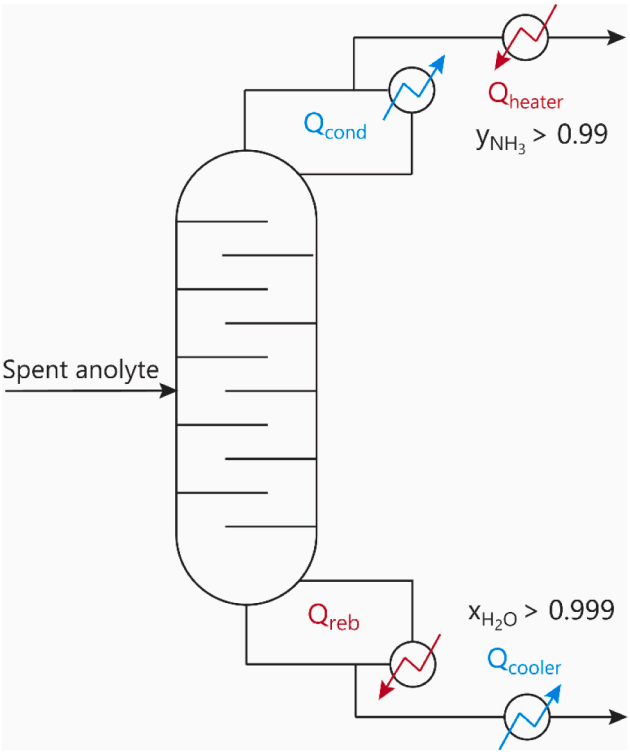

Fig. 1. Schematic of HYSYS distillation column model used for sub-atmospheric and atmospheric simulations.

Because the distillation column is modelled as a continuous process, the duties of each heating and cooling unit are calculated in units of power. This power was converted to energy using the volumetric flow rate to compare it to the energy output of the battery through the following equation

$$E_{tot} = \frac{\sum Q_i}{\dot{V}} \tag{5}$$

where E_{tot} is the total energy requirement of the column (normalized to Wh L^{-1} of anolyte), Q_i is the power of each component (reboiler, condenser, distillate heater, and bottoms cooler), and $\dot{V}$ is the flow rate into the distillation column [8]. To compare the energy requirement of just the units that use waste heat to the total column energy, Eq. (5) was modified to only include the power requirement of the reboiler and ammonia heater as

$$E_{heat} = \frac{Q_{reb} + Q_{heater}}{\dot{V}} \tag{6}$$

where E_{heat} is the heat energy requirement of the column (normalized to Wh L^{-1} of anolyte), Q_{reb} is the power of the reboiler and Q_{heater} is the power of the ammonia heater. The flow rate was 1 L s^{-1} to be consistent with the most recent TRAB thermal regeneration publication [32], but by using Eqs. (5) and (6), the analysis becomes independent of flow rate since the power requirement of the column scales linearly with flow rate.

To establish theoretical limits of the Cu_{aq}-TRAB system, the theoretical energy density of the discharge process and the thermal recharging energy density requirements were used to estimate cycle energy efficiencies. The theoretical energy density was calculated using values and methods from a previous publication [28], with the solubility limit of copper changing with the ammonia concentration. The total energy efficiency and efficiency relative to Carnot were evaluated as,

$$\eta_{tot} = \frac{\hat{u}}{E_{tot}}, \text{ and } \eta_{\frac{tot}{carnot}} = \frac{\eta_{tot}}{1 - \frac{T_C}{T_H}}, \tag{7,8}$$

where η_{tot} is the total energy efficiency, $\hat{u}$ is the theoretical energy density of the discharge processes, $\eta_{tot/carnot}$ is the efficiency relative to Carnot, T_C is the cold temperature, and T_H is the hot temperature [8,28]. Similar to Eq. (5), Eq. (7) and (8) were modified to only account for heating units. Consequently, the equations were modified to use E_{heat} instead of E_{tot} as

$$\eta_{heat} = \frac{\hat{u}}{E_{heat}}, \text{ and } \eta_{\frac{heat}{carnot}} = \frac{\eta_{heat}}{1 - \frac{T_C}{T_H}}, \tag{9,10}$$

where η_{heat} is energy efficiency relative to the reboiler and ammonia heater and $\eta_{heat/carnot}$ is the efficiency relative to Carnot for the same thermal units. For the sub-atmospheric column, $T_C = 23$ °C and $T_H = 70$ °C, resulting in a Carnot efficiency of 13.7%. For the atmospheric column, $T_C = 23$ °C and $T_H = 100$ °C, resulting in a Carnot efficiency of 20.6%. The condenser and reboiler temperatures used here are consistent with previous investigations and reboiler temperatures are similar to recently published experimental values that analyzed the impact of electrolyte concentration on the solution vapor pressure [31,32].

3. Results and discussion

3.1. Battery sensitivity analysis

Experimental full cell tests and model results showed that the peak power of the Cu_{aq}-TRAB increased by 14% as the operating temperature increased from 25 to 50 °C (Fig. 2). The peak power density at 50 °C was 22 mW cm^{-2}, which is among the highest reported values for a single-metal TRB system reported. Most of the increase was attributed to 15% lower ohmic resistance of the cell from the elevated temperature. Gains in power were despite a 30 mV decrease in open circuit potential

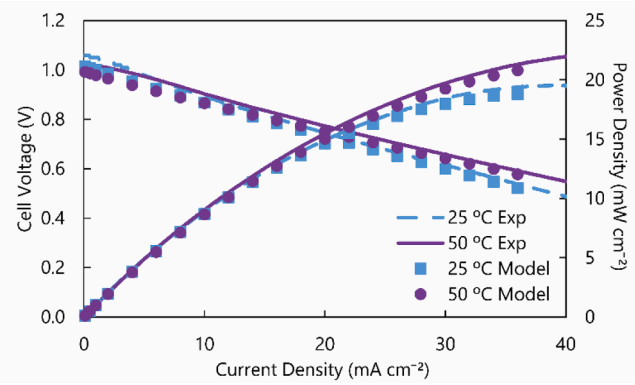

Fig. 2. Comparison of model and experimental polarization/power curves at two operating temperatures with a flow rate of 50 mL min^{-1}.

which occurred due to the standard potential of the negative electrode increasing with temperature more than the positive electrode (Table 3). The numerical model accurately replicated the experimental polarization curve, with the open circuit potential, polarization curve slope, and therefore peak power density being <5% different.

The sensitivity analysis at 25 °C showed that ohmic contributions had the largest impact on battery performance (Fig. 3). The baseline peak power density was 17.1 mW cm^{-2}, the peak power density for low and high membrane conductivity were 14.2 and 19.9 mW cm^{-2}, and the peak power densities at 10 and 50 mL min^{-1} were 15.8 and 18.6 mW cm^{-2}. Changes in the exchange current density resulted in a change of peak power density <0.05 mW cm^{-2}, likely due to the very fast reaction rate of the Cu(I/II) redox couple [27] and high active surface area of the porous carbon electrode [45]. Therefore, even if catalysts or alternative ligands were used to increase the reaction rate, there would be no change in battery performance. While the change in peak power due to flow rate was half that of the change in peak power due to membrane conductivity, when comparing the percent change in power to the percent change in the independent variable, membrane conductivity contributes significantly more than flow rate. The flowrate varied from −50% to +150% from the baseline case but only resulted in an 8% change in peak power. For the ±20% change in the membrane conductivity, there was a ±16% change in peak power relative to the baseline. Therefore, when normalizing the change in peak power to the percent change in the independent variable, membrane conductivity had roughly eight times the impact of flow rate. These findings are consistent with previous TRAB investigations that show large ohmic losses in the battery [13,20], and that flow rate has a diminishing impact

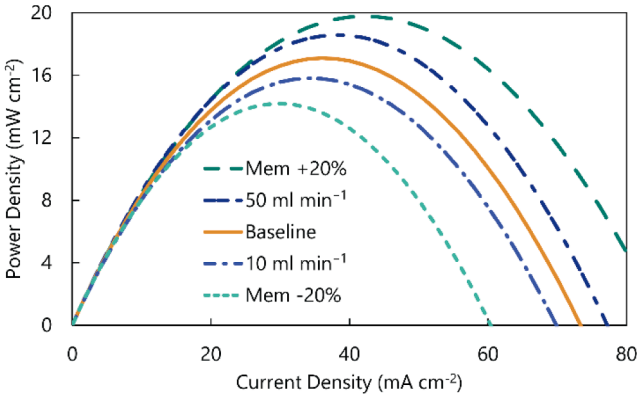

Fig. 3. Sensitivity of power density curves to membrane conductivity and flow rate at 25 °C. Baseline parameters are 20 mL min^{-1} and all other values as measured experimentally. Sensitivity to exchange current density is not shown because change was negligible compared to baseline.

on power density as it is increased [21,46,47]. These results demonstrate that future Cu_{aq}-TRAB studies should focus on minimizing ohmic losses in the system to improve battery performance, and this is likely to extend to other TRABs given the similar nature of the battery chemistries.

Because of the outsized impact of membrane conductivity at 25 °C, only the sensitivity to membrane conductivity was investigated for elevated temperature battery operation. The baseline peak power densities were 18.0 and 18.8 mW cm^{-2} at 50 and 75 °C (Fig. 4) because the membrane conductivity increased more at elevated temperature than the open circuit potentiall decreased (Fig. S3). At 50 °C, the low and high peak power densities were 15.1 and 20.7 mW cm^{-2}, and at 75 °C the low and high peak power densities were 15.7 and 21.5 mW cm^{-2}. These changes in peak power density were 15% and 14% at 50 and 75 °C, suggesting that even as temperature and therefore conductivity increased, the ohmic losses were still the dominant contribution to battery performance. Experimental discharge curves showed that there was little change in energy density at elevated temperature battery operation (Fig. S4). It was expected that at elevated temperature diffusive transport of NH_3 would increase, resulting in an energy loss, but this was likely offset by higher membrane conductivity and lower ohmic losses. While reducing ammonia transport is a pertinent issue in TRABs [18,48], reduction of ohmic losses can also result in significant performance improvements even if ammonia transport is similar. As shown by these results, there is little drawback to battery operation at elevated temperatures since higher power can be achieved with minimal energy losses. Future work that increases energy density by controlling ammonia crossover at room temperature should directly carry over to elevated temperature operation. The energy used to heat the battery could come from the waste heat stream that is already in use by the TRAB system but could also come from the stack itself since large-scale flow battery stacks are known to produce heat and require cooling and thermal management.

3.2. Thermal recharging

The total column energy requirement generally decreased as the inlet stream temperature increased, until a critical temperature was reached (Fig. 5a and b). For the sub-atmospheric column, the minimum column energy occurred at 56, 49, and 48 °C for ammonia concentrations of 1, 3, and 5 M, respectively (Fig. 5a). After the minimum duty was reached, the column energy increased due to the ammonia purity in the distillate decreasing, causing an increase in condenser duty to keep the ammonia at the required purity specification. The low ammonia concentration consistently had the lowest column energy requirement; however, the difference between the energy requirement at 1 and 5 M NH_3 was lowest at their respective optimal inlet temperatures. The total column energy was less sensitive to ammonia concentration when operating at atmospheric pressure (Fig. 5b). For low ammonia concentrations, the minimum column energy was at the highest inlet temperature studied (75 °C), and for 5 M NH_3, the optimal inlet temperature was 71 °C. Atmospheric column pressure resulted in higher total column duty, but despite this, sub-atmospheric column operation may not be worth the lower energy requirement since the column will have more complex design and operation [32].

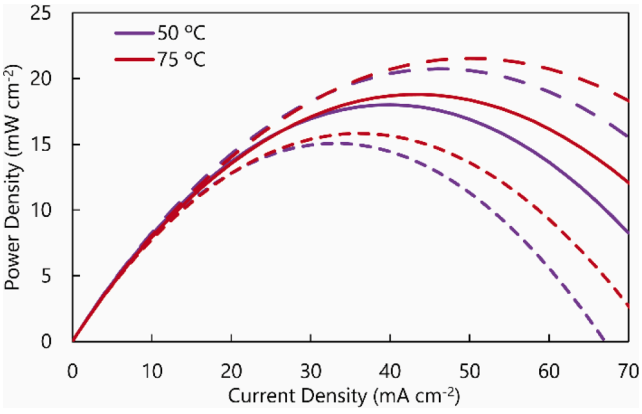

Fig. 4. Sensitivity of power density curves to membrane conductivity at 50 and 75 °C. Baseline parameters are 20 mL min^{-1} and all other values as measured experimentally. Solid lines represent baseline, long dashes represent + 20% conductivity, and short dashes represent −20% conductivity.

The reboiler and condenser consumed the majority of the energy for both column pressures analyzed (Fig. 5c and d). Generally, the ammonia heater required the smallest energy input because of the low weight percent of ammonia (~10%) even at the highest concentration studied. For the sub-atmospheric column, the contributions of the reboiler and condenser each represented about 40 % of the energy input, while at atmospheric pressure, the reboiler contributed 57% of the total energy requirement. This resulted in the atmospheric column having a much higher E_{heat} than the sub-atmospheric column with a heating to cooling ratio of 2.4:1 for the column (Table S1). Further reduction of the total energy requirement could be achieved with additional engineering of the system. For example, the cold, pure ammonia stream and hot bottoms stream could be run countercurrent in a heat exchanger, reducing the total column energy requirement by as much as 3.6–7.4% (double the contribution of the ammonia heater). The highest theoretical total energy efficiency was 5.5% at sub-atmospheric and 5.0% at atmospheric pressure, corresponding to efficiencies relative to Carnot of 40.1% and 24.3% (see Table S1 for more detailed values). The highest theoretical heat efficiency was 12.2% at sub-atmospheric and 8.6% at atmospheric pressure, corresponding to efficiencies relative to Carnot of 88.7% and 41.7%. No previous TRB investigation has previously defined these limits, and this demonstrates that the Cu_{aq}-TRAB has the potential to achieve much higher efficiencies with performance improvements.

While high ammonia concentrations increased the total energy required for the thermal recharging step, the higher discharge capacity of the battery (caused by higher copper solubility) compensated for these increases resulting in higher efficiencies (Fig. 6a and b). The sub-atmospheric column efficiency relative to Carnot was significantly higher because the energy requirement of the reboiler of this column was much lower and the temperature drop across the column was low. At face value, this would indicate that the sub-atmospheric column would be preferred due to the more efficient utilization of the waste heat stream, but the inverse is likely to be the case. The primary reason that TRABs are designed to use low temperature heat as the input energy source is because the low temperature heat is a very cheap energy source, especially in comparison to whatever electrical energy is used for the condenser and bottoms cooler. Therefore, it would likely be more prudent to operate the column at atmospheric pressure because it uses more waste heat compared to expensive cooling energy, despite the column using the waste heat less efficiently. It is then recommended that future TRAB reports use E_{heat} at 1 atm for system evaluation because it is the most representative value and use of non-waste heat energy could potentially be minimized further.

Experimentally, the Cu_{aq}-TRAB has produced efficiencies of around 2% at the maximum, which is well below the theoretical maximums presented in this work due to inefficiencies in the electrochemical cell (Fig. 7). As demonstrated in **Section 3.1**, ohmic losses dominate battery performance, thus exploring methods to minimize ohmic losses such as alternative membranes and thinner electrodes could be beneficial for efficiency by increasing realizable energy outputs. Prevention of energy losses due to crossover has also been shown to increase battery performance and this can be accomplished though better transport control and decreasing free ammonia concentration, but thus far methods to do this have only increased ohmic losses. These results also demonstrate the ease in which reported performance metrics can change simply by using different battery and system results that, despite being pertinent

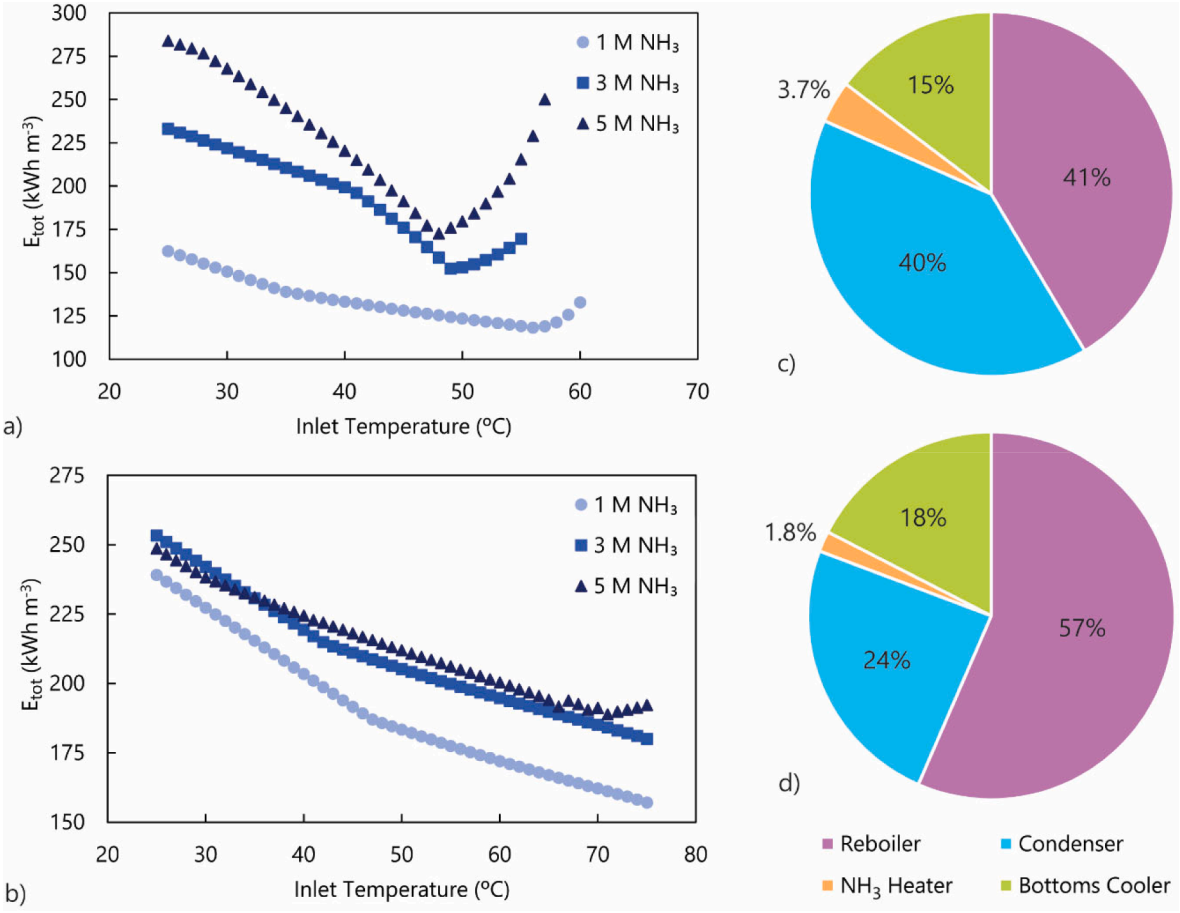

Fig. 5. Total column duty at various temperatures and ammonia concentrations for a) sub-atmospheric column and b) atmospheric column. Breakdown of contributions of each individual thermal unit to total energy at minimum column duty and 5 M NH_3 concentration for c) sub-atmospheric column and d) atmospheric column.

considerations and technology advancements, can misrepresent actual system performance gains. For example, the data could be underrepresented by using average power density and E_{tot} at 1 atm (Fig. 7, **Point 1**), or overrepresented by using peak power density and E_{heat} at 0.24 atm (Fig. 7, **Point 4**). While the battery can be operated at peak power (Fig. 7, **Point 3**), this is unlikely to be done if the system were to be installed on the grid due to high overpotentials decreasing the amount of energy that can be discharged. Therefore, the most appropriate conditions for reporting TRAB metrics would be the average power density and E_{heat} at 1 atm (Fig. 7, **Point 2**), as this is the most similar metric to the rated power of a grid-scale flow battery. This is well below the current peak power density and theoretical efficiency limit (Fig. 7, **red star**), demonstrating that there is potential for significant future development of the Cu_{aq}-TRAB.

3.3. Integration with natural gas turbine system

TRBs have been proposed as technologies to be coupled with systems that are already in operation and producing waste heat in order to extract additional power and energy out of the waste streams of the system. Natural gas turbines are one of such systems that are commonly used on the grid for power production and are stationary systems that produce a large amount of low-temperature heat that is not used by the system. As an example, a Solar Turbines Taurus 60 turbine produces 6.15 MW of power when averaging over the whole year (Fig. S5a). Given that the exhaust temperature is over 500 °C (Fig. S5b), the heat exchanger between the turbine fluid and the Cu_{aq}-TRAB anolyte would have a small footprint. While any device could be scaled to produce a certain amount of power, the size of the device is a pertinent metric to consider because practical implementation of new technologies is limited by capital cost and geographic footprint. Per a recent review, system power density and efficiency are the two most critical metrics for waste heat technologies [3]. Basic calculations were done to estimate the size of the Cu_{aq}-TRAB that would be needed to produce 1% of the power of the turbine (61.5 kW). To scale the Cu_{aq}-TRAB, an average power density of 6 mW cm^{-2}, a 40 × 40 cm electrode stack [49,50] and 4.5 mm of thickness to account for the electrodes, flow fields and bipolar plates were used. This analysis does not consider auxiliary equipment for either system, but rather uses the perspective of just the power generation systems. For these conditions, the electrodes would take up 9.2 m^3 of space or about 4.0% of the size of the Taurus 60 turbine (229 m^3). If the system were designed to store approximately 2.5 Wh L^{-1}, and therefore 61.5 kWh of energy, it would require 49.2 m^3 of total electrolyte in two reservoir tanks. With improvements in ohmic losses to the point where the peak power density (22 mW cm^{-2}) becomes the average power density, the total size of the electrodes would be reduced to 2.5 m^3, or 1.1% of the volume of the turbine. If the theoretical maximum energy density (9.5 Wh L^{-1}) can be achieved, the total volume of electrolytes would be 13.0 m^3.

4. Conclusions

Membrane resistance was found to be the dominant source of performance loss in the Cu_{aq}-TRAB system, and therefore, future research to minimize ohmic losses in the Cu_{aq}-TRAB should be the focus to improve battery performance. Based on our 3D model, there was a 15% response

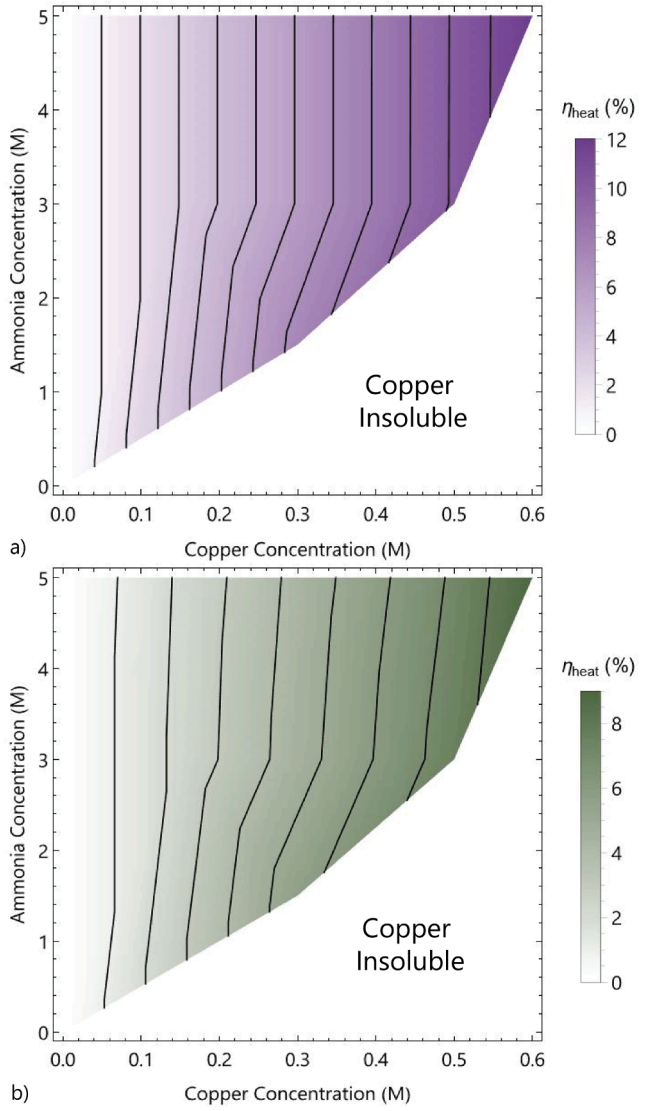

Fig. 6. Contour plots showing heat efficiency for a range of copper and ammonia concentrations at a) 0.24 atm and b) 1 atm of column pressure. Each contour line represents 1% efficiency.

in peak power density when the membrane conductivity was changed by ±20% for operating temperatures ranging from 25 to 75 °C. Peak power density increased to 21.5 mW cm^2 at 75 °C and a flow rate of 20 mL min^{-1} when the membrane conductivity was 20% above the experimentally predicted value. For the first time, theoretical efficiency limits were estimated for any TRB by a systematic study of distillation column operation at different temperatures, pressures, and ammonia concentrations. The theoretical efficiency limit of the Cu_{aq}-TRAB system was estimated to be 8.6% when using 5 M NH_3 and operating the distillation column at atmospheric pressure. It was estimated that current capabilities of the Cu_{aq}-TRAB would require a geometric footprint of 9.2 m^3 for power production and 49.2 m^3 for energy storage but could be reduced to 2.5 m^3 and 13.0 m^3 given advancements in minimizing ohmic losses and controlling parasitic ammonia transport.

CRediT authorship contribution statement

Nicholas R. Cross: Methodology, Investigation, Visualization, Validation. **Matthew J. Rau:** Conceptualization, Supervision, Methodology, Writing – review & editing. **Serguei N. Lvov:** Methodology, Supervision, Writing – review & editing. **Christopher A. Gorski:** Methodology, Writing – review & editing. **Bruce E. Logan:** Conceptualization, Methodology, Writing – review & editing. **Derek M. Hall:** Funding acquisition, Supervision, Conceptualization, Methodology, Writing – review & editing.

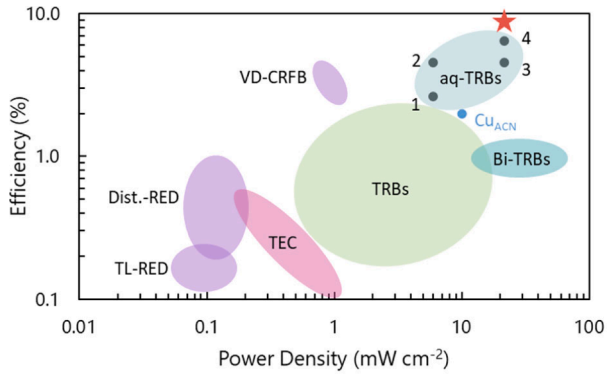

Fig. 7. Comparison of efficiency of power density for results from this work and other previous waste heat utilization systems [4]. Demonstration of range where a single technology could fall on the plot depending on which performance metrics are published. 1 – average power density, total efficiency at 1 atm; 2 – average power density, heat efficiency at 1 atm; 3 – peak power density, heat efficiency at 1 atm; 4 – peak power density, total efficiency at 0.24 atm. Star represents current peak power density and theoretical heat efficiency limit at 1 atm column pressure. Abbreviations: TL-RED = Thermolysis Reverse Electrodialysis, Dist.-RED = Distillation Reverse Electrodialysis, TEC = Thermoelectrochemical Cell, VD-CRFB = Vacuum Distillation Concentrated Redox Flow Battery, TRBs = single metal Thermally Regenerative Batteries, Bi-TRBs = bimetallic TRBs, aq-TRBs = this work.

Declaration of Competing Interest

The authors declare the following financial interests/personal relationships which may be considered as potential competing interests: [Derek M. Hall reports financial support was provided by US Department of Energy. Derek M. Hall has patent All aqueous thermally-regenerative battery pending to The Penn State Research Foundation.].

Data availability

Data will be made available on request.

Acknowledgements

This material is based upon work supported by the Department of Energy under Award Number DE-FE0032030. The authors would like to thank Erica Winegardner for providing the natural gas turbine data readouts.

Appendix A. Supplementary material

Supplementary data to this article can be found online at https://doi.org/10.1016/j.apenergy.2023.120959.

References

[1] Firth A, Zhang B, Yang A. Quantification of global waste heat and its environmental effects. Appl Energy 2019;235:1314–34. https://doi.org/10.1016/j.apenergy.2018.10.102.
[2] Orr B, Singh B, Tan L, Akbarzadeh A. Electricity generation from an exhaust heat recovery system utilising thermoelectric cells and heat pipes. Appl Therm Eng 2014;73:588–97. https://doi.org/10.1016/j.applthermaleng.2014.07.056.
[3] Brogioli D, La Mantia F. Innovative technologies for energy production from low temperature heat sources: critical literature review and thermodynamic analysis. Energy Environ Sci 2021:1057–82. https://doi.org/10.1039/d0ee02795b.

[4] Brogioli D, La Mantia F. Electrochemical methods for exploiting low-temperature heat sources: challenges in material research. Adv Energy Mater 2022:12. https://doi.org/10.1002/aenm.202103842.

[5] Huo D, Tian H, Shu G, Wang W. Progress and prospects for low-grade heat recovery electrochemical technologies. Sustain Energy Technol Assessments 2022;49:101802. https://doi.org/10.1016/j.seta.2021.101802.

[6] Battistel A, Peljo P. Recent trends in thermoelectrochemical cells and thermally regenerative batteries. Curr Opin Electrochem 2021;30:100853. https://doi.org/10.1016/j.coelec.2021.100853.

[7] Cheng C, Dai Y, Yu J, Liu C, Wang S, Feng SP, et al. Review of liquid-based systems to recover low-grade waste heat for electrical energy generation. Energy Fuel 2021. https://doi.org/10.1021/acs.energyfuels.0c03733.

[8] Rahimi M, Straub AP, Zhang F, Zhu X, Elimelech M, Gorski CA, et al. Emerging electrochemical and membrane-based systems to convert low-grade heat to electricity. Energy Environ Sci 2018;11:276–85. https://doi.org/10.1039/c7ee03026f.

[9] Rahimi M, D'Angelo A, Gorski CA, Scialdone O, Logan BE. Electrical power production from low-grade waste heat using a thermally regenerative ethylenediamine battery. J Power Sources 2017;351:45–50. https://doi.org/10.1016/j.jpowsour.2017.03.074.

[10] Peljo P, Lloyd D, Doan N, Majaneva M, Kontturi K. Towards a thermally regenerative all-copper redox flow battery. Phys Chem Chem Phys 2014;16:2831–5. https://doi.org/10.1039/c3cp54585g.

[11] Maye S, Girault HH, Peljo P. Thermally regenerative copper nanoslurry flow batteries for heat-to-power conversion with low-grade thermal energy. Energy Environ Sci 2020;13:2191–9. https://doi.org/10.1039/d0ee01590c.

[12] Kratochvil B, Betty KR. A secondary battery based on the copper(II)-(I) and (I)-(0) couples in acetonitrile. J Electrochem Soc 1974;121:851. https://doi.org/10.1149/1.2401935.

[13] Palakkal VM, Nguyen T, Nguyen P, Chernova M, Rubio J, Venugopalan G, et al. A high power thermally regenerative ammonia-copper redox flow battery enabled by a zero gap cell design, low-resistant membranes and electrode coatings. ACS Appl Energy Mater 2020. https://doi.org/10.1021/acsaem.0c00400.

[14] Vicari F, Galia A, Scialdone O. Development of a membrane-less microfluidic thermally regenerative ammonia battery. Energy 2021;225:120221. https://doi.org/10.1016/j.energy.2021.120221.

[15] Zhang F, Liu J, Yang W, Logan BE. A thermally regenerative ammonia-based battery for efficient harvesting of low-grade thermal energy as electrical power. Energy Environ Sci 2015;8:343–9. https://doi.org/10.1039/c4ee02824d.

[16] Tian H, Jiang W, Shu G, Wang W, Huo D, Shakir MZ. Analysis and optimization of thermally-regenerative ammonia-based flow battery based on a 3-D model. J Electrochem Soc 2019;166:A2814–5. https://doi.org/10.1149/2.0711912jes.

[17] Zhang Y, Shi Y, Zhang L, Li J, Fu Q, Zhu X, et al. Graphene oxide modified membrane for alleviated ammonia crossover and improved electricity generation in thermally regenerative batteries. Chinese Chem Lett 2022;34:107704. https://doi.org/10.1016/j.cclet.2022.07.047.

[18] Lu Z, Shi Y, Zhang L, Li Y, Li J, Fu Q, et al. Ammonia crossover in thermally regenerative ammonia-based batteries for low-grade waste heat recovery. J Power Sources 2022;548:232085. https://doi.org/10.1016/j.jpowsour.2022.232085.

[19] Zhang Y, Shi Y, Zhang L, Li J, Fu Q, Zhu X, et al. A fluidized-bed reactor for enhanced mass transfer and increased performance in thermally regenerative batteries for low-grade waste heat recovery. J Power Sources 2021;495:229815. https://doi.org/10.1016/j.jpowsour.2021.229815.

[20] Rahimi M, Kim T, Gorski CA, Logan BE. A thermally regenerative ammonia battery with carbon-silver electrodes for converting low-grade waste heat to electricity. J Power Sources 2018;373:95–102. https://doi.org/10.1016/j.jpowsour.2017.10.089.

[21] Cross NR, Hall DM, Lvov SN, Logan BE, Rau MJ. The impact of fiber arrangement and advective transport in porous electrodes for silver-based thermally regenerated batteries. Electrochim Acta 2021;388:138527. https://doi.org/10.1016/j.electacta.2021.138527.

[22] Wang W, Tian H, Shu G, Huo D, Zhang F, Zhu X. A bimetallic thermally regenerative ammonia-based battery for high power density and efficiently harvesting low-grade thermal energy. J Mater Chem A 2019;7:5991–6000. https://doi.org/10.1039/c8ta10257k.

[23] Wang W, Shu G, Tian H, Huo D, Zhu X. A bimetallic thermally-regenerative ammonia-based flow battery for low-grade waste heat recovery. J Power Sources 2019;424:184–92. https://doi.org/10.1016/j.jpowsour.2019.03.086.

[24] Wang W, Tian H, Huo D, Yang S, Li S, Zhu X, et al. Modelling of a bimetallic thermally-regenerative ammonia flow battery for conversion efficiency and performance evaluation. J Power Sources 2021;499:229943. https://doi.org/10.1016/j.jpowsour.2021.229943.

[25] Wang W, Huo D, Tian H, Zhu X, Shu G. Temperature characteristics of a copper/zinc thermally-regenerative ammonia battery. Electrochim Acta 2020;357:136860. https://doi.org/10.1016/j.electacta.2020.136860.

[26] Wang W, Yang S, Huo D, Tian H, Li S, Zhu X, et al. Understanding the reaction mechanism and self-discharge of a bimetallic thermally-regenerative ammonia battery. Electrochim Acta 2021;370:137724. https://doi.org/10.1016/j.electacta.2021.137724.

[27] Springer R, Cross NR, Lvov SN, Logan BE, Gorski CA, Hall DM. An all-aqueous thermally regenerative ammonia battery chemistry using Cu(I, II) redox reactions. J Electrochem Soc 2021;168:070523. https://doi.org/10.1149/1945-7111/ac1030.

[28] Cross NR, Rau MJ, Lvov SN, Gorski CA, Logan BE, Hall DM. Power and energy capacity tradeoffs in an all-aqueous copper thermally regenerative ammonia battery. J Power Sources 2022;531:231339. https://doi.org/10.1016/j.jpowsour.2022.231339.

[29] Zhang F, LaBarge N, Yang W, Liu J, Logan BE. enhancing low-grade thermal energy recovery in a thermally regenerative ammonia battery using elevated temperatures. ChemSusChem 2015;8:1043–8. https://doi.org/10.1002/cssc.201403290.

[30] Vicari F, D'Angelo A, Kouko Y, Loffredi A, Galia A, Scialdone O. On the regeneration of thermally regenerative ammonia batteries. J Appl Electrochem 2018;48:1381–8. https://doi.org/10.1007/s10800-018-1240-0.

[31] Luo J, Wang Z, Wu H, Zhang S. Vapor pressure measurement of electrolyte solution and its impact on regeneration process in TRAB. Case Stud Therm Eng 2022;36:102201. https://doi.org/10.1016/j.csite.2022.102201.

[32] Engelpracht M, Kohrn M, Tillmanns D, Seiler J, Bardow A. waste heat to power: full-cycle analysis of a thermally regenerative flow battery. Energy Technol 2022;2200152:2200152. https://doi.org/10.1002/ente.202200152.

[33] Nield D, Bejan A. Convection in Porous Media. 3rd ed. Springer; 2006.

[34] Newman J, Balsara N. Electrochemical Systems. 4th ed. Englewood Cliffs: Wiley; 2021.

[35] Lvov SN. Introduction to Electrochemical Science and Engineering. 2nd ed. Boca Raton: CRC Press; 2021.

[36] Himmelblau DM. Diffusion of dissolved gases in liquids. Chem Rev 1964;64:527–50. https://doi.org/10.1021/CR60231A002.

[37] Zaytsev ID, Aseyev GG. Properties of Aqueous Solutions of Electrolytes. CRC Press; 1992.

[38] Hall DM, Grenier J, Duffy TS, Lvov SN. The energy storage density of redox flow battery chemistries: a thermodynamic analysis. J Electrochem Soc 2020;167:110536. https://doi.org/10.1149/1945-7111/aba4e2.

[39] Yue G, Zhao L, Olvera OG, Asselin E. Speciation of the H2SO4-Fe2(SO 4)3-FeSO4-H2O system and development of an expression to predict the redox potential of the Fe3 +/Fe 2 + couple up to 150 °c. Hydrometall 2014;147–148:196–209. https://doi.org/10.1016/j.hydromet.2014.05.008.

[40] Zhou X, Zhang X, Lv Y, Lin L, Wu Q. Nano-catalytic layer engraved carbon felt via copper oxide etching for vanadium redox flow batteries. Carbon N Y 2019;153:674–81. https://doi.org/10.1016/j.carbon.2019.07.072.

[41] Jiang B, Wu L, Yu L, Qiu X, Xi J. A comparative study of Nafion series membranes for vanadium redox flow batteries. J Memb Sci 2016;510:18–26. https://doi.org/10.1016/j.memsci.2016.03.007.

[42] Rahimi M, Schoener Z, Zhu X, Zhang F, Gorski CA, Logan BE. Removal of copper from water using a thermally regenerative electrodeposition battery. J Hazard Mater 2017;322:551–6. https://doi.org/10.1016/j.jhazmat.2016.10.022.

[43] AspenTech. Aspen HYSYS 2021.

[44] Zhu X, Rahimi M, Gorski CA, Logan B. A thermally-regenerative ammonia-based flow battery for electrical energy recovery from waste heat. ChemSusChem 2016;9:873–9. https://doi.org/10.1002/cssc.201501513.

[45] González-García J, Bonete P, Expósito E, Montiel V, Aldaz A, Torregrosa-Maciá R. Characterization of a carbon felt electrode: Structural and physical properties. J Mater Chem 1999;9:419–26. https://doi.org/10.1039/a805823g.

[46] Shi Y, An Y, Tang Z, Zhang L, Li J, Fu Q, et al. Electrical power production of thermally regenerative ammonia-based batteries using reduced graphene oxide modified Ni foam composite electrodes. Appl Energy 2022;326:119966. https://doi.org/10.1016/j.apenergy.2022.119966.

[47] Zhang Y, Zhang L, Li J, Zhu X, Fu Q, Liao Q, et al. Performance of a thermally regenerative ammonia-based flow battery with 3D porous electrodes: Effect of reactor and electrode design. Electrochim Acta 2020;331:135442. https://doi.org/10.1016/j.electacta.2019.135442.

[48] Wang W, Shu G, Zhu X, Tian H. Decoupled electrolytes towards enhanced energy and high temperature performance of thermally regenerative ammonia batteries. J Mater Chem A 2020;8:12351–60. https://doi.org/10.1039/d0ta03236k.

[49] Kim S, Thomsen E, Xia G, Nie Z, Bao J, Recknagle K, et al. 1 kW/1 kWh advanced vanadium redox flow battery utilizing mixed acid electrolytes. J Power Sources 2013;237:300–9. https://doi.org/10.1016/j.jpowsour.2013.02.045.

[50] Guarnieri M, Trovò A, D'Anzi A, Alotto P. Developing vanadium redox flow technology on a 9-kW 26-kWh industrial scale test facility: design review and early experiments. Appl Energy 2018;230:1425–34. https://doi.org/10.1016/j.apenergy.2018.09.021.